Review of Scientific Instruments

Inter-satellite laser link acquisition with dual-way scanning for Space Advanced Gravity Measurements mission

Cite as: Rev. Sci. Instrum. **89**, 064501 (2018); https://doi.org/10.1063/1.5019433
Submitted: 14 December 2017 . Accepted: 10 May 2018 . Published Online: 01 June 2018

Jing-Yi Zhang, Min Ming, Yuan-Ze Jiang, Hui-Zong Duan, and Hsien-Chi Yeh

Inter-satellite laser link acquisition with dual-way scanning for Space Advanced Gravity Measurements mission

Jing-Yi Zhang,[1] Min Ming,[1] Yuan-Ze Jiang,[1] Hui-Zong Duan,[2,3] and Hsien-Chi Yeh[2,3,a)]
[1]*MOE Key Laboratory of Fundamental Physical Quantities Measurement, School of Physics, Huazhong University of Science and Technology, 1037 Luo Yu Road, Wuhan 430074, China*
[2]*Tianqin Research Center for Gravitational Physics, Sun Yat-sen University, Zhuhai Campus, Zhuhai 519000, China*
[3]*School of Physics and Astronomy, Sun Yat-sen University, Zhuhai Campus, Zhuhai 519000, China*

(Received 14 December 2017; accepted 10 May 2018; published online 1 June 2018)

Laser link acquisition is a key technology for inter-satellite laser ranging and laser communication. In this paper, we present an acquisition scheme based on the differential power sensing method with dual-way scanning, which will be used in the next-generation gravity measurement mission proposed in China, called Space Advanced Gravity Measurements (SAGM). In this scheme, the laser beams emitted from two satellites are power-modulated at different frequencies to enable the signals of the two beams to be measured distinguishably, and their corresponding pointing angles are determined by using the differential power sensing method. As the master laser beam and the slave laser beam are decoupled, the dual-way scanning method, in which the laser beams of both the master and the slave satellites scan uncertainty cones simultaneously and independently, can be used, instead of the commonly used single-way scanning method, in which the laser beam of one satellite scans and that of the other one stares. Therefore, the acquisition time is reduced significantly. Numerical simulation and experiments of the acquisition process are performed using the design parameters of the SAGM mission. The results show that the average acquisition time is less than 10 s for a scanning range of 1-mrad radius with a success rate of more than 99%. *Published by AIP Publishing.*
https://doi.org/10.1063/1.5019433

I. INTRODUCTION

Due to high coherence and directionality, the laser has been an essential tool for performing precision measurements and communication over a large inter-satellite distance in space-based science missions, e.g., GRACE (Gravity Recovery and Climate Experiment) Follow-On,[1] SAGM,[2] LISA (Laser Interferometer Space Antenna),[3] and TianQin.[4] Laser link acquisition is the first step to build inter-satellite laser links for science missions with satellite formation flying. Various laser link acquisition strategies have been proposed in space missions.[5–9] The beacon light and charge coupled devices (CCDs) are usually implemented as a coarse beam pointing to reduce the acquisition time because of their wide field-of-view. Two acquisition schemes without using the beacon and CCD have been proposed for the GRACE Follow-On-type mission.[10–14] The acquisition strategies are accomplished by using the quadrant photodiode (QPD) to detect the heterodyne signal and power signal, respectively. The optimal pointing angle is obtained when the maximum-strength signal is recorded after scanning over the whole uncertainty cone sequentially. The total acquisition times for the initial line-of-sight calibration of these two schemes are several hours and 160 s, respectively.

We attempt to develop an inter-satellite laser link acquisition scheme in which the acquisition system can be embedded in the laser ranging system and realize the miniaturization of the terminal with lower power consumption for the SAGM mission. The SAGM mission is designed for the Earth's gravity recovery mission, similar to the GRACE Follow-On mission. The proposed inter-satellite distance of SAGM is 100–200 km with an altitude of approximately 400 km. The transponder-type laser ranging system with heterodyne optical phase locking, instead of homodyne phase locking proposed in the original mission concept, will measure the inter-satellite distance changes. The noise level of inter-satellite ranging is 10 nm/Hz$^{1/2}$ at 0.1 Hz. The simplified layout of the laser ranging system is shown in Fig. 1. The laser beam, emitted from the fiber collimator of the master laser, passes through the polarizing beam-splitter (PBS). Most of the light is reflected by the PBS and the cube-corner retro-reflector; the reflected light later propagates over a large inter-satellite distance to the slave satellite. The light emitted from the slave laser is superimposed with the received light on the PBS and later passes through the imaging system. After passing through the beam splitter, the transmitted light arrives at QPD2 directly to generate the beat signal. For a transponder inter-satellite laser ranging system, the beat signal is used for the range and range-rate measurements, as well as the differential wavefront sensing (DWS).[15,16] The reflected light passing through a focusing lens is detected by QPD1. The focusing lens is used to convert the angle of the beam axis to the position of the focal spot on the QPD. This position signal will be used for laser link acquisition. The basic parameters of the laser ranging system are listed in Table I.

a)Author to whom correspondence should be addressed: yexianji@mail.sysu.edu.cn

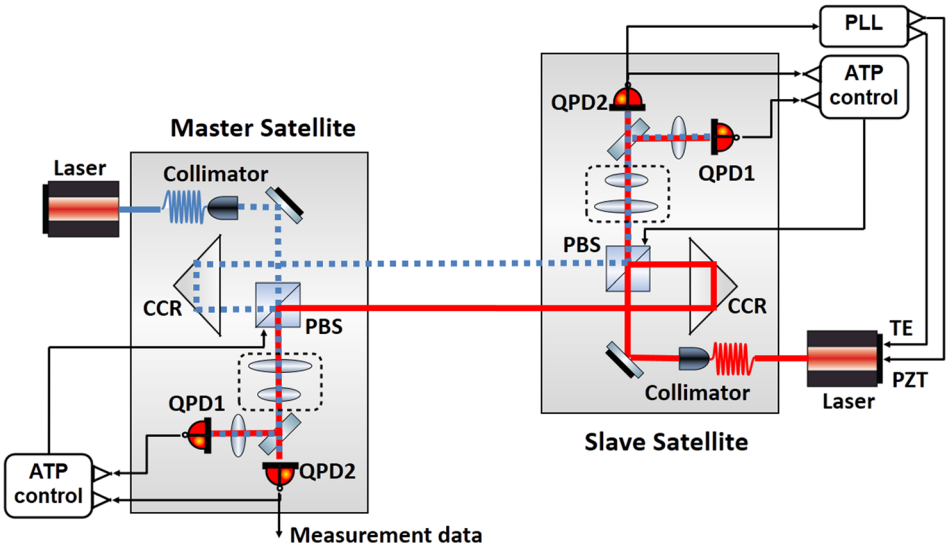

FIG. 1. A simplified layout of the laser ranging system. PLL: phase locked loop; ATP: acquisition, tracking, and pointing; TE and PZT represent the thermal control and the piezoelectric control channels for frequency tuning of the slave laser, respectively; the lens group in the dotted frame is the imaging system; CCR represents the cube-corner retro-reflector, which is used to reflect the beam backward along the incident beam axes.

The basic principle of the DWS method is to determine the relative wavefront misalignment between two beams by measuring the phase differences on the receiving plane of the QPD. The precision phase measurement requires a high signal-to-noise ratio and an interference signal with a suitable beat frequency; however, the initial misalignment of laser link, i.e., the unknown offset between the line of sight and the beam axis of the laser ranging system, may be around milli-radian, primarily caused by the assembly tolerances and misalignments during launch.[11] Typically, the deflection exceeding 300 μrad will make the signal below the noise level. Moreover, the initial frequency difference between the master laser and the slave laser may be up to 1-2 GHz, as the bandwidth of photodiode is only approximately 20 MHz. Therefore, the laser link acquisition must take into account five degrees of freedom (DoFs), including two rotational DoFs for each satellite and the frequency of the slave laser. The boundaries formed by the initial maximum offsets of the misalignment angle and the frequency difference are the values of the uncertainty cones.

The coupling of five degrees of freedom will lead to a long acquisition time. It is expected that a shorter acquisition time can be achieved by decoupling the spatial and frequency acquisition processes and the dual-way scanning, which is exactly the merit of differential power sensing (DPS).

TABLE I. Parameters of the laser ranging system.

Parameter	Variable	Typical value
Satellite separation (km)	z	200
Laser wavelength (nm)	λ	1064
Loss in the optical path	ε	0.2
Transmitted power (W)	P	1
Local beam power (μW)	P_{local}	10
Local beam waist (mm)	ω_0	2.5
Received aperture radius (mm)	R	4
Photodiode responsivity (A/W)	ρ_{PD}	0.68

II. PRINCIPLE

In the acquisition scheme we propose, the powers of the master laser and the slave laser are modulated at different frequencies within the photodiode's bandwidth to allow the signals of the master and slave laser beams to be distinguished after demodulation. Thus, the dual-way scanning method in which the laser beams of both the master and the slave satellites scan uncertainty cones simultaneously and independently can be used. The PBS on both the master and slave satellites is steering along a specifically defined scan track to control the transmitted beam scanning over the area of the spatial uncertainty cone at the same time. Once one satellite captures enough power of the laser beam emitted from the other satellite, the scanning process is stopped immediately and the beam angle signal measured by the DPS method is used as a control signal to auto-lock the pointing of the transmitted beam until the transmitted beam and received beam are parallel. Because a spherical wavefront is expected after a long-distance propagation, the axis of the received beam can be regarded as the line of sight. At this time, the other satellite will also receive enough power. The process is repeated until both satellites lock their beams to the line of sight. Figure 2 shows the principle of the beam alignment process. The first figure shows the ideal situation in which the received beam and transmitted beam are aligned. Both the local and received beams are imaged at the center of the QPD after passing through the PBS and the focusing lens. The second figure shows the situation that the alignment changes, leading to a misalignment between the received and transmitted beam. In this situation, the imaging spot of the received beam is no longer located in the center of the QPD, and an error signal is generated. Through a proportional-integral-derivative (PID) controller, the PBS, which is driven by a fast steering mirror, will be rotated to make the error signal of the DPS approach zero. As a result, the transmitted beam is accordingly parallel to the received beam and points back to the other satellite, as shown in the last figure.

Once the spatial acquisition is completed, the frequency of the slave laser is tuned until the frequency interval is within

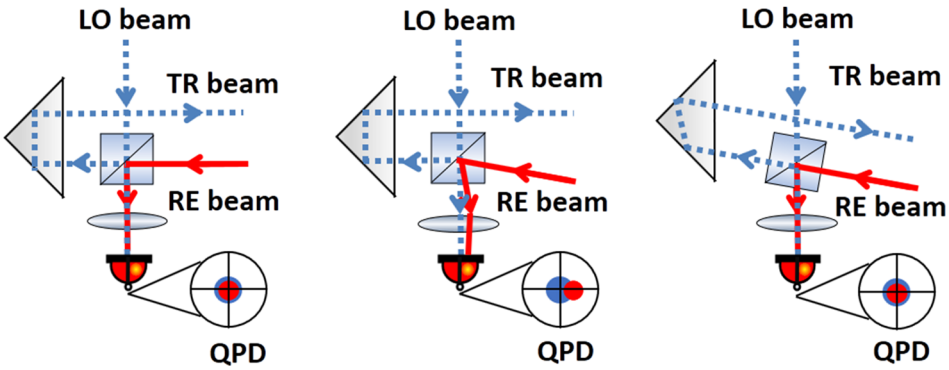

FIG. 2. Working principle of the beam alignment process. The LO beam, the RE beam, and the TR beam represent the local beam, the received beam, and the transmitted beam, respectively.

the locking range of the laser frequency auto-locking system. The details of the laser frequency auto-locking are given in Ref. 17. After the laser frequency is locked and the phasemeter and interferometer are working, the DWS will take over the control of the PBS for ultra-precision beam pointing and tracking.

It is obvious that the fewer the DoFs of the signal detected for acquisition are coupled, the shorter the acquisition time is. The spatial and frequency acquisitions are decoupled by detecting the laser power; the spatial acquisitions of the master and the slave lasers are decoupled by modulating the laser beam powers at different frequencies, which helps to reduce the acquisition time significantly. Moreover, during the process of beat frequency tuning, the misalignment angles can be kept in auto-locking mode to avoid the failure in frequency acquisition caused by a beam jitter. Due to a short acquisition time required, the re-acquisition after the loss of the signal can be completed in the same way as the initial acquisition.

A. Power modulation

According to Table I, the effective received power after power modulation can be expressed as

$$\tilde{P}_i = \frac{1}{2}[1 + \cos(2\pi f_i t)]P_i, \tag{1}$$

$$P_i = (1-\varepsilon)\frac{2P}{\pi}\frac{1}{\omega^2(z)}\exp(-2\frac{(\alpha_i{}^2+\beta_i{}^2)z^2}{\omega^2(z)})\cdot\pi R^2, \tag{2}$$

$$\omega(z) = \omega_0\sqrt{1+(\frac{\lambda z}{\pi\omega_0{}^2})^2}, \tag{3}$$

where i refers to the master laser or the slave laser and α and β are the tilt-angles in the pitch and yaw directions, respectively. Accordingly, the maximum received power for acquisition is approximately 17 nW.

After the sampling and demodulating processes, the voltage signals of the received and local beams on the four quadrants can be obtained. Thus, we can estimate the beam angle by using the following equations:[18]

$$\theta \approx \frac{x}{f} = \frac{\pi r}{4f}\cdot\frac{V_A+V_C-(V_B+V_D)}{V_A+V_B+V_C+V_D}, \tag{4}$$

$$\Delta\theta \approx \frac{1.22\pi\lambda}{4R}\cdot\frac{S_{noise}}{\rho_{PD}P_i}, \tag{5}$$

where $V_{A,B,C,D}$ are the output voltages of the QPD, x is the distance between the spot center and the QPD center, r is the spot radius on the surface of the QPD, and f = 50 mm is the focal distance. According to the formula, we know that for a position error of the QPD of x = 1 μm, the pointing error is approximately 2×10^{-5} rad. The position error of the QPD can be eliminated by subtracting the positions of the received and the local beams. The dominant noise sources of this method are the equivalent current noise of the photodiode, the laser relative intensity noise, and the shot noise from the local laser because the power of the local beam is much stronger than that of the received beam. Table II summarizes the noise budget of the angle measurement. According to Eq. (5), the beam angle measurement noise is approximately 4×10^{-7} rad/Hz$^{1/2}$, which meets the requirement for the spatial acquisition of SAGM.

The amplitude calculation in the experiment is based on the cross-correlation method,[19] which is realized by using a data acquisition card with 16-bit resolution and a sampling frequency of 100 kHz; N = 5000 is the number of data sampled for a period of integration. To avoid the non-integral-cycle sampling,[20] harmonics, and low-frequency noise, the modulating frequencies are set to be 900 Hz and 1500 Hz. Therefore, the standard deviation of the total noise of four photodiode segments is approximately 0.2 nA for 20 Hz data updating frequency, which is much smaller than that of the received signal (11.5 nA).

B. Scanning pattern

The hexagonal scan pattern is an efficient and common coverage of the plane with a circle, as shown in Fig. 3.[10] It is a discrete stepping scan that is suitable for scanning-responding detection.

The dwell time T_d is determined by the operation time of demodulation, the closed-loop feedback control of the steering mirror, and the inter-satellite propagation time of the laser beam; θ_{FOV} and θ_{step} are the radii of the uncertainty cone and the scan step, respectively. According to the scan track, the total time for scanning over the whole uncertainty area can be

TABLE II. Main noise sources of the single QPD segment.

Noise source	Variable	Typical value (pA/Hz$^{1/2}$)
Laser relative intensity noise	S_i	17
Shot noise	S_s	1
Equivalent current noise	S_e	2
Total noise	S_{noise}	17.1

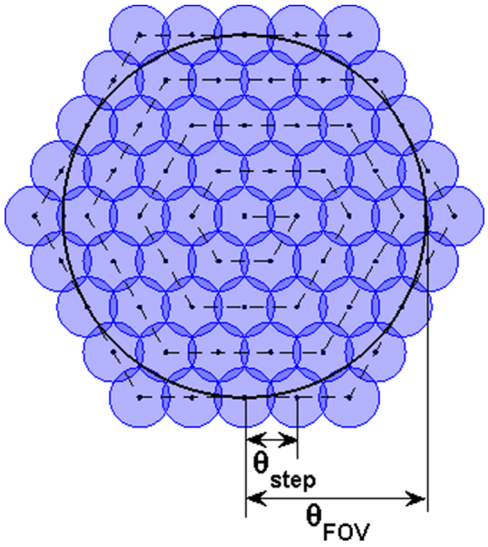

FIG. 3. Hexagonal scan.

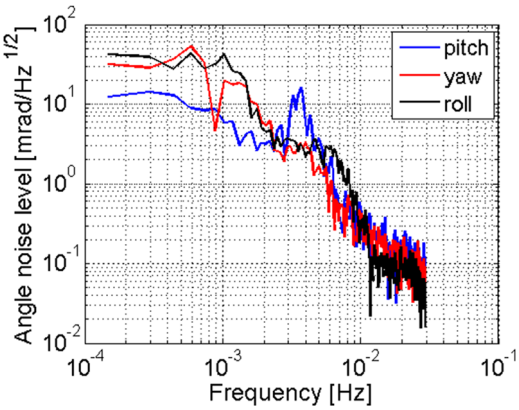

FIG. 4. Power spectral density of the jitter.

estimated by

$$T_{total} = (6 \cdot \frac{\left\lceil \frac{2\theta_{FOV}}{\sqrt{3}\theta_{step}} \right\rceil \left(\left\lceil \frac{2\theta_{FOV}}{\sqrt{3}\theta_{step}} \right\rceil + 1 \right)}{2} + 1) \cdot T_d$$
$$= (3 \left\lceil \frac{2\sqrt{3}\theta_{FOV}}{3\theta_{step}} \right\rceil^2 + 3 \left\lceil \frac{2\sqrt{3}\theta_{FOV}}{3\theta_{step}} \right\rceil + 1) \cdot T_d. \quad (6)$$

It is obvious that a larger scan step results in a shorter acquisition time. However, the scan step depends on the value of threshold, which determines whether a valid signal can be received.

III. SIMULATION

Simulation is compulsory for optimizing the key parameters of acquisition; these parameters strongly depend on the initial misalignment and the jitter that cause different effects on the received laser beam and the emitted laser beam. For the satellite emitting a Gaussian laser beam, the misalignment causes a change in the power, but not in the phase, received at the target satellite. This is due to the fact that a spherical wavefront is expected after a long-distance propagation. By contrast, for the satellite receiving the laser beam, the misalignment causes a change in the received phase but not in the received power. We consider these above-mentioned effects in the simulation of the acquisition process with a 200-km inter-satellite distance.

The acquisition process is realized as a discrete time-domain simulation and is simulated by using the Opto-Sim software developed based on Matlab® and Simulink®. The simulation parameters are set as the typical values mentioned above. The initial misalignment is modeled as Gaussian distribution in pitch and yaw. The jitter is modeled according to the data of GRACE;[21] the power spectral density of the jitter is shown in Fig. 4. Considering the technical specifications of the steering mirror used in the experiments, the radius of the spatial uncertainty cone is set to be 1 mrad.

Based on the statistics of 1000 simulation results, the relations of the success rate and the average acquisition time varying with the scan step are shown in Fig. 5. Because of the measurement noise mentioned before, the thresholds are set to be 0.2–0.3 to ensure a good margin. The dwell time is set to be 0.5 s. The solid lines refer to the dual-way scanning, and the dashed lines refer to the single-way scanning. The results show that the performance of the dual-way scanning is better than that of the single-way scanning for the same acquisition parameters.

Figure 6 shows typical time evolutions of the intersecting angles between the beam axes and the line of sight and the received laser power in the master and slave satellites measured by QPD1, respectively, during the dual-way scanning process with the optimized parameters.

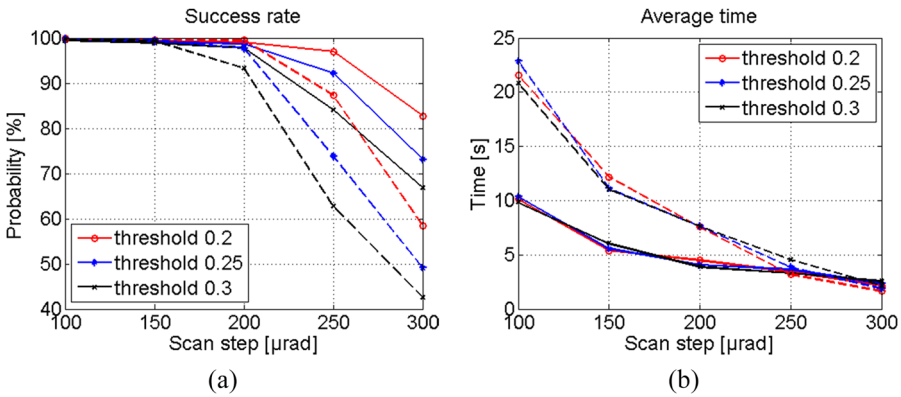

FIG. 5. Success rate and average time of spatial acquisition vary with the scan step. The solid lines refer to dual-way scanning, and the dashed lines refer to single-way scanning. The threshold is in units of the maximum laser power received that is about 17 nW in this simulation.

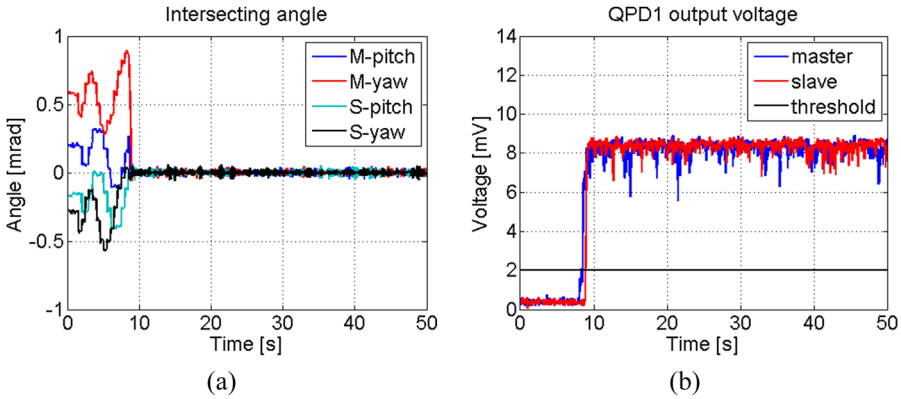

FIG. 6. Time evolutions of spatial acquisition. (a) The intersecting angles between the beam axes and the line of sight. (b) The output voltages of QPD1 of the master satellite and the slave satellite.

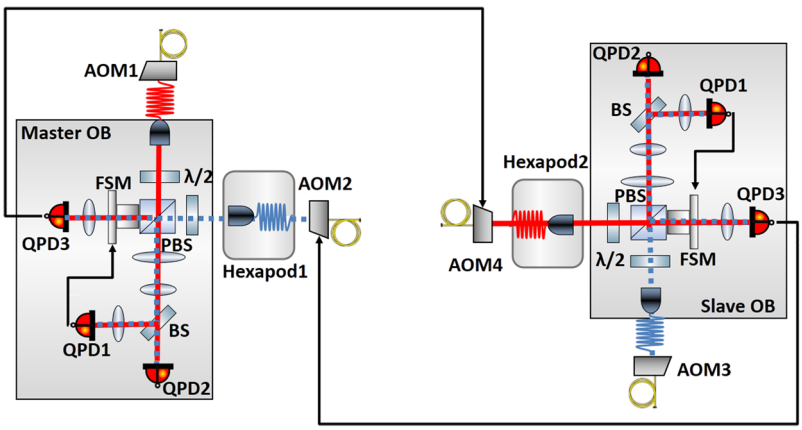

FIG. 7. Setup of the acquisition experiment.

IV. PROTOTYPE AND EXPERIMENTAL RESULTS

A. Experiment setup

To test the validity and performance of the acquisition algorithm, a ground-based simulation system for inter-satellite laser link acquisition has been built. The 200-km beam propagation and the misalignments are simulated by changing the received laser power and the wavefront of the received beam. The experimental setup is shown in Fig. 7. Since the laser frequency is irrelevant to the DPS method, the Doppler frequency shift corresponding to the relative speed between the two satellites is unnecessary to be considered. A Nd:YAG laser with an optical power of 250 mW is used as the light source. The functions of the acousto-optic modulators (AOMs) are (1) to modulate the laser power for beam labeling, which is required for dual-way scanning with DPS and (2) to attenuate the laser power for simulating the received power fluctuation caused by misalignment. The laser beams modulated by AOM1 and AOM3 are the local beams of the master satellite and the slave satellite, respectively. The laser beams modulated by AOM2 and AOM4 are the received beams of the master satellite and the slave satellite, respectively. Accordingly, the modulation frequencies of AOM1 and AOM4 are the same (as labeling the master laser beams), either is the modulation frequencies of AOM2 and AOM3. Moreover, the tilts of the wavefront of the received beam caused by misalignment are simulated by Hexapod1 and Hexapod2 for the master satellite and the slave satellite, respectively.

The local beam and received beam are superimposed on the PBS, which is held by a triple-PZT-driven fast steering mirror (FSM) with a 10 mm clear aperture that allows laser

TABLE III. Parameters of the optical power.

Parameter	Typical value
Local beam power on QPD1 (μW)	10
Received beam power on QPD1 (nW)	17
Local beam power on QPD2 (μW)	10
Received beam power on QPD2 (nW)	17
Local beam power on QPD3 (μW)	2
Received beam power on QPD3 (μW)	8

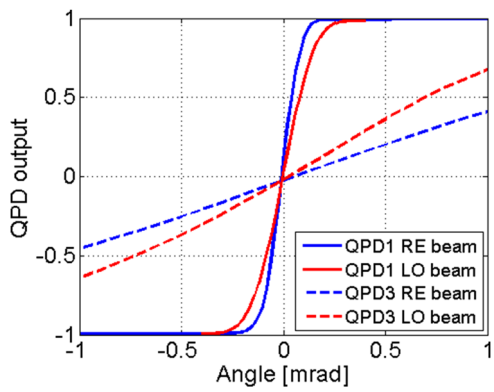

FIG. 8. Calibration curves of the QPDs. LO beam and RE beam represent the local beam and received beam, respectively.

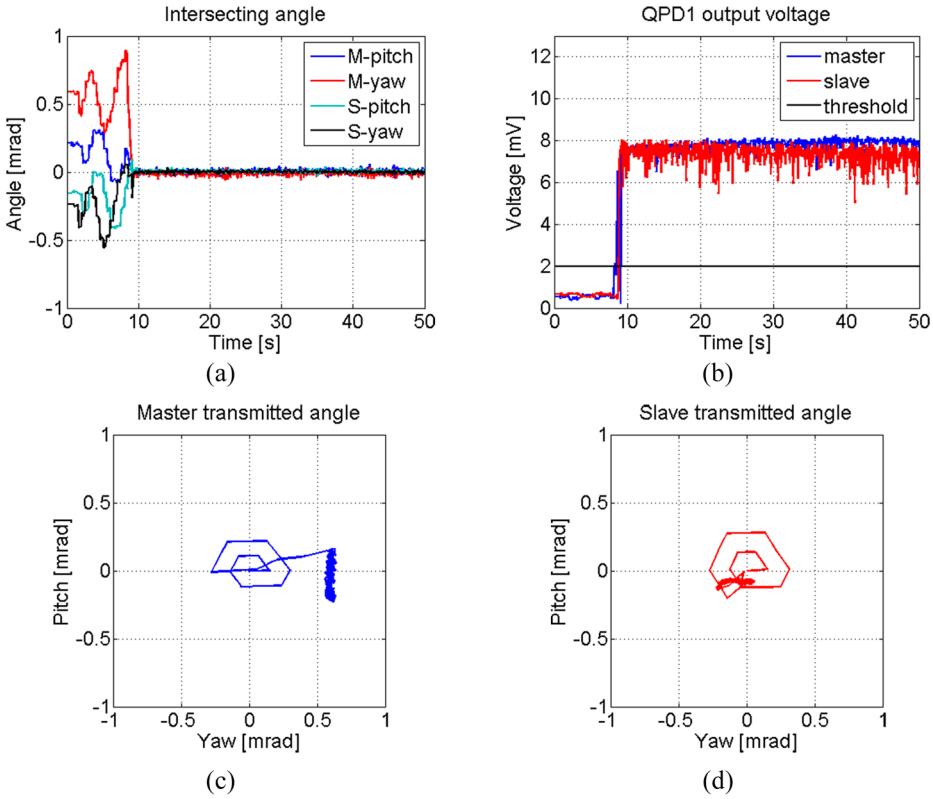

FIG. 9. Time evolutions of spatial acquisition. (a) The intersecting angles between the beam axes and the line of sight. (b) The output voltages of QPD1 of the master satellite and the slave satellite. (c) The track of the master transmitted angle. (d) The track of the slave transmitted angle.

beams to pass through it. Subsequently, the mixed beam is divided into two parts by a 50:50 beam splitter: one part is focused and detected by QPD1 for DPS, and the other part is detected by QPD2 for the interference signal.

To simulate the actual power attenuation and fluctuation caused by a 200-km inter-satellite distance and the misalignment of the laser link, the misalignment angle between the transmitted beam and the line of sight measured by QPD3 is fed to the controller of the power modulation of AOM4, to link to the slave satellite. The same feedback control of power modulation is also followed for AOM2. The $\lambda/2$ wave plate is used to adjust the optical power on the QPDs in the alignment state, as shown in Table III, to ensure that QPD3 can detect the received beam signal during the simulation process.

B. Results

To calibrate the beam angle measurement of the QPDs, the hexapods are driven to create a 20-μrad stepping angular motion. Figure 8 shows the calibration curves of QPDs. The sensitivities of the received beam and the local beam on QPD1 are 1.12×10^4/rad and 6.82×10^3/rad, respectively. The linear range of the received beam for DPS is approximately ± 60 μrad. The sensitivities of the received beam and the local beam on QPD3 are 4.43×10^2/rad and 6.91×10^2/rad, respectively, and the nonlinearity is approximately 30 μrad in the range of 0.8 mrad, that is, 3.75%.

To demonstrate the acquisition process, we conduct a simulation experiment with dual-way dynamically spatial acquisition. The random motions for simulating the misalignment are applied to Hexapod1 and Hexapod2. We repeat the process many times with different initial misalignments and jitters to verify the feasibility of the laser link acquisition strategy.

The parameters are set to be the same as those in the numerical simulation. Figure 9(a) shows the time evolution of the intersecting angles between the beam axes and the line of sight, and Fig. 9(b) shows the time evolution of the received laser power in the master and slave satellites measured by QPD3 and QPD1, respectively. Figures 9(c) and 9(d) show the tracks of the master and slave transmitted angles measured by QPD3. At $t = 9$ s, the pointing angle is locked and kept for a time that is sufficiently long to complete the laser frequency acquisition. The experimental results are consistent with the numerical simulation results.

V. CONCLUSIONS

An automatic laser link acquisition scheme based on differential power sensing has been designed for the SAGM mission. In the proposed scheme, to avoid the failure caused by an unexpected jitter, laser power modulation/demodulation is used to label the master laser beam and the slave laser beam, so that the dual-way scanning can be implemented, and the acquisition time can be reduced further. Numerical simulation and experiments are carried out to optimize the acquisition parameters and to verify the feasibility of the acquisition scheme. The results indicate that the spatial acquisition can be accomplished within an average time of 10 s for a 1-mrad uncertainty cone.

ACKNOWLEDGMENTS

This work is supported by the National Natural Science Foundation of China (Grant Nos. 11655001 and 11654004).

[1]B. S. Sheard, G. Heinzel, K. Danzmann, D. A. Shaddock, W. M. Klipstein, and W. M. Folkner, J. Geod. **86**, 1083 (2012).
[2]H. C. Yeh, Q. Z. Yan, Y. R. Liang, Y. Wang, and J. Luo, Rev. Sci. Instrum. **82**, 044501 (2011).
[3]K. Danzmann and A. Rüdiger, Classical Quantum Gravity **20**, S1–S9 (2003).
[4]J. Luo, L. S. Chen, H. Z. Duan, Y. G. Gong, S. C. Hu, J. H. Ji, Q. Liu, J. W. Mei, M. Vadim, S. Mikhail, C. G. Shao, T. Viktor, H. B. Tu, Y. M. Wang, Y. Wang, H. C. Yeh, M. S. Zhan, Y. H. Zhang, Z. Vladimir, and Z. B. Zhou, Classical Quantum Gravity **33**, 035010 (2016).
[5]T. Tolker-Nielsen and G. Oppenhauser, Proc. SPIE **4635**, 1–16 (2002).
[6]R. Lange and B. Smutny, Proc. SPIE **5712**, 1–12 (2005).
[7]T. Jono, Y. Takayama, N. Kura, K. Ohinata, Y. Koyama, K. Shiratama, Z. Sodnik, B. Demelenne, A. Bird, and K. Arai, Proc. SPIE **6105**, 610503 (2006).
[8]P. G. Maghami, T. T. Hyde, and J. Kim, Classical Quantum Gravity **22**, S421–S428 (2005).
[9]F. Cirillo and P. F. Gath, J. Phys.: Conf. Ser. **154**, 012014 (2009).
[10]C. Mahrdt, "Laser link acquisition for the GRACE follow-on laser ranging interferometer," Ph.D. thesis, Max-Planck-Institute for Gravitational Physics, Albert Einstein Institute, 2014.
[11]D. M. R. Wuchenich, C. Mahrdt, B. S. Sheard, S. P. Francis, R. E. Spero, J. Miller, C. M. Mow-Lowry, R. L. Ward, W. M. Klipstein, G. Heinzel, K. Danzmann, D. E. McClelland, and D. A. Shaddock, Opt. Express **22**, 11351–11366 (2014).
[12]J. Sanjuan, M. Gohlke, S. Rasch, K. Abich, A. Görth, G. Heinzel, and C. Braxmaier, Appl. Opt. **54**, 6682–6689 (2015).
[13]Z. Luo, Q. Wang, C. Mahrdt, A. Goerth, and G. Heinzel, Appl. Opt. **56**, 1495–1500 (2017).
[14]F. Ales, P. Gath, U. Johann, and C. Braxmaier, in *AIAA Guidance, Navigation, and Control Conference* (AIAA, 2015), p. 0094.
[15]E. Morrison, B. J. Meers, D. I. Robertson, and H. Ward, Appl. Opt. **33**, 5041–5049 (1994).
[16]G. Heinzel, V. Wand, A. García, O. Jennrich, C. Braxmaier, D. Robertson, K. Middleton, D. Hoyland, A. Rüdiger, R. Schilling, U. Johann, and K. Danzmann, Classical Quantum Gravity **21**, S581–S587 (2004).
[17]Y. Luo, H. Li, and H. C. Yeh, Rev. Sci. Instrum. **87**, 056105 (2016).
[18]L. M. Manojlović, Appl. Opt. **50**, 3461–3469 (2011).
[19]Y. R. Liang, H. Z. Duan, H. C. Yeh, and J. Luo, Rev. Sci. Instrum. **83**, 095110 (2012).
[20]J. L. Roberts, in *IEEE International Conference on Acoustics, Speech and Signal Processing (ICASSP)* (IEEE, 1978), Vol. 3, pp. 674–677.
[21]T. Bandikova, J. Flury, and U. D. Ko, Adv. Space Res. **50**, 123–135 (2012).